

# 3D-RBSM ANALYSIS OF DEEP BEAM FAILED IN SHEAR

Y. Hanifi GEDIK<sup>\*1</sup>, Hikaru NAKAMURA<sup>\*2</sup>, Yoshihito YAMAMOTO<sup>\*3</sup> and Minoru KUNIEDA<sup>\*4</sup>

## ABSTRACT

The behavior of deep beams failed in shear with shear span ratio ( $a/d$ ) of 0.5 was investigated using 3D-RBSM, which is a representative method of discrete method. The analytical results for the beam without web reinforcement were compared with the experimental ones and analysis capability of 3D-RBSM was confirmed. 3D effects were discussed by comparing the change of strut widths and high stress as well as 3D deformed shapes. Then, the effect of web reinforcement was investigated. It was confirmed that, there is no significant effect of web reinforcement in deep beams with  $a/d=0.5$ .

**Keywords:** Rigid-Body-Spring-Model, deep beam, shear failure, 3D effect, web reinforcement

## 1. INTRODUCTION

Numerical simulation of the shear failure behavior of RC deep beams is one of the difficult problems in concrete structures, since it is complex and affected by several cases such as shear crack propagation, bond and anchorage of rebar and compression failure of concrete. The major numerical tool for concrete structures is Finite Element Method (FEM) that based on continuum mechanics. However, the failure of concrete structures shows discontinuous behavior. Particularly, the failure localizes near loading and support points with complex stress state in deep beams. Unreasonable behavior such as instability problem has been observed when the localization behavior is simulated by FEM due to inconsistency with continuum mechanics. On the other hand, numerical models based on discrete mechanics such as Rigid-Body-Spring-Model (RBSM) have been proposed and applied to concrete structures. Firstly, it was proposed by Kawai [1]. RBSM can provide realistic behavior from cracking to failure. It can also investigate stress transfer mechanism in meso levels [2].

In this study, pre- and post-peak behavior of deep beams failed in shear with  $a/d=0.5$  are investigated three-dimensionally in detail using 3-D RBSM. The experimental work of Kosa and others [3,4] is applied to the numerical analysis. Numerical results such as load-displacement curve and crack pattern are compared with the experimental ones and the applicability of RBSM is discussed. Afterwards, three-dimensional behavior in deep beams failed in shear is investigated using the analytical results by comparing the strut widths and stress values on the middle and surface longitudinal section.

Furthermore, deep beams with web reinforcement are analyzed and compared with the no

web reinforcement case in order to determine the effect of web reinforcement for  $a/d=0.5$  case.

## 2. ANALYTICAL METHOD

### 2.1 Three-Dimensional RBSM

In 3-D RBSM, concrete is modeled as an assemblage of rigid particles interconnected by springs along their boundaries. Continuum mechanics assures the internal behavior of each particle. On the other hand, the response of the spring model provides insight of the interaction between the particles instead. Each rigid particle has three translational and three rotational degrees of freedom defined at the nuclei (Figure 1.a). As shown in the figure, the boundary surface of two particles is divided by several triangles with the center of gravity and vertices of the surface. The integral point has one normal and two tangential springs. This model can automatically evaluate the effect of bending and torsional moment without setting any rotational springs [2].

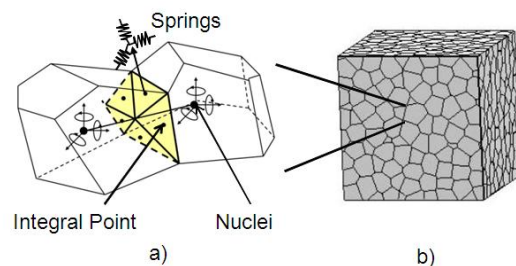


Fig.1 a) Rigid Body Spring Model b) Voronoi Diagram

The crack pattern is strongly affected by the mesh design since the cracks initiate and propagate through interface boundaries of particles. A random

\*1 Graduate School of Engineering, Nagoya University, JCI Member

\*2 Prof., Dept. of Civil Engineering, Nagoya University, Dr.E., JCI Member

\*3 Assistant Prof., Dept. of Civil & Environmental Engineering, National Defense Academy, JCI Member

\*4 Associate Prof., Dept. of Civil Engineering, Nagoya University, Dr.E., JCI Member

geometry of rigid particles is generated by Voronoi diagram (Figure 1.b), which reduces the mesh bias on the initiation and propagation of potential cracks [5].

A series of beam elements is used in order to model the reinforcement that can be established independently not depending the concrete discretization [6]. Each beam-node has two translational and one rotational degree of freedom. The load transfer between these beam nodes and concrete particles are provided by linkage elements that provide the connection between beam elements and particles [7].

## 2.2 Concrete Model

Figure 2 shows the concrete models used in RBSM [2]. The tensile model of normal spring is  $\frac{1}{4}$  tensile model shown in Figure 2.a. The model considers the tensile fracture energy.

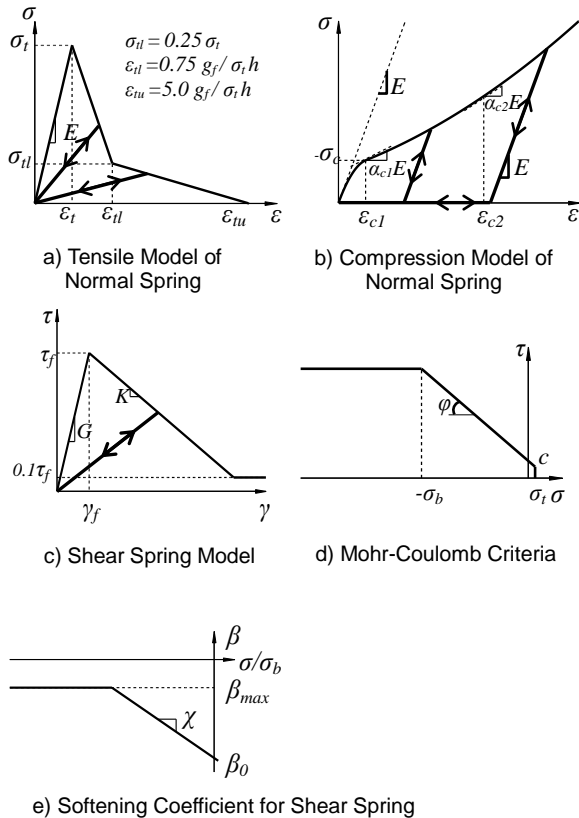


Fig. 2 Concrete Models

The compression model of the normal spring is given in Figure 2.b. Two functions given in equation 1 constitute this model.

$$\sigma = \begin{cases} a_0 \varepsilon^2 + b_0 \varepsilon & (\varepsilon > \varepsilon_{c1}) \\ a_1 \varepsilon^2 + b_1 \varepsilon + c_1 & (\varepsilon \leq \varepsilon_{c1}) \end{cases} \quad (1)$$

$\varepsilon_{c1}$ ,  $a_0$ ,  $b_0$ ,  $a_1$ ,  $b_1$  and  $c_1$  in the equation are obtained by parametric analyses and the values used in the analyses are given in Table 1.

Table 1 Parameters for Concrete Model

Parameters	$f_c' = 36.2$ MPa	$f_c' = 30.0$ MPa
$\varepsilon_{c1}$	$-2.26 \times 10^{-3}$	$-2.00 \times 10^{-3}$
$a_0$ (MPa)	$7.89 \times 10^6$	$8.34 \times 10^6$
$b_0$ (MPa)	$4.19 \times 10^4$	$3.92 \times 10^4$
$a_1$ (MPa)	$-1.64 \times 10^{+5}$	$-1.51 \times 10^{+5}$
$b_1$ (MPa)	$5.54 \times 10^{+3}$	$5.28 \times 10^{+3}$
$c_1$ (MPa)	$-4.10 \times 10^{+1}$	$-3.39 \times 10^{+1}$
$\beta_0$	-0.05	-0.05
$\beta_{max}$	-0.025	-0.025
$\chi$	-0.01	-0.01

The shear spring model is shown in Figure 2.c. In the model, two tangential springs are combined. Equation 2 gives the shear strain where  $\gamma_l$  and  $\gamma_m$  are strains of each spring. The stress for each spring is calculated by equation 3.

$$\gamma = \sqrt{\gamma_l^2 + \gamma_m^2} \quad (2)$$

$$\tau_l = \tau (\gamma_l / \gamma), \quad \tau_m = \tau (\gamma_m / \gamma) \quad (3)$$

The stress elastically increases up to the shear strength with the slope of shear modulus ( $G$ ). Figure 2.d shows Mohr-Coulomb type criteria for shear. In shear spring model,  $K$  is the slope of softening part that is obtained by equation 4 where  $\beta$  is obtained from Figure 2.e. The shear stress in the model decreases by increase of crack width.

$$K = \beta G \quad (4)$$

Compressive failure of normal spring does not occur in this model. However, it was confirmed that the compressive failure behavior can be simulated with confinement effect by combination of normal spring and shear springs.

Figure 3 shows the stress-strain relationship obtained from the simulation of uniaxial compression test of concrete for specimen B2, B2-S, B3-S and B4-S, which are explained in the next chapter.

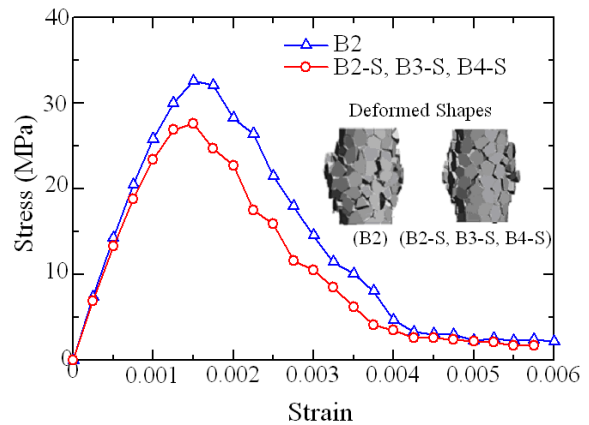


Fig. 3 Stress-Strain Relationship and Deformed Shapes of Uniaxial Compression Tests

### 3. OVERVIEW OF ANALYZED SPECIMENS

Analyses are carried out for four deep beams that are B2, which is a tested specimen by Kosa and others [3,4], B2-S, B3-S and B4-S having shear span ratio of 0.5. The specimens of B2 and B2-S have no web reinforcement in shear span (Figure 4) where B3-S and B4-S have web reinforcement ratio of 0.4% and 0.8% in shear span given in Figure 5 and 6 respectively. Table 2 shows the properties for all specimens.

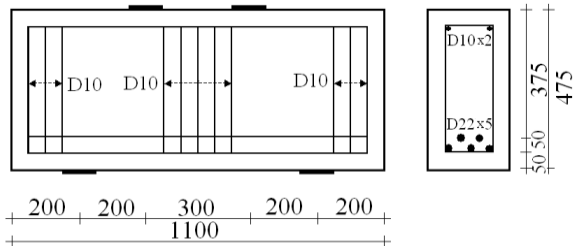


Fig. 4 Deep Beam B2 and B2-S ( $a/d=0.5$ )

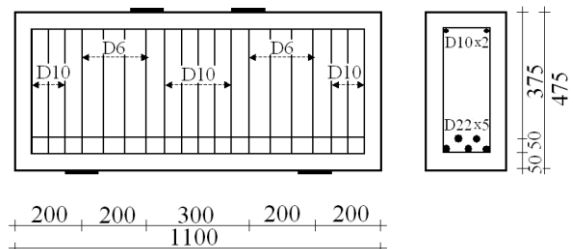


Fig. 5 Deep Beam B3-S ( $a/d=0.5$ )

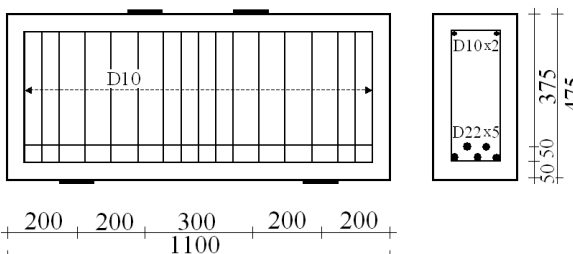


Fig. 6. Deep Beam B4-S ( $a/d=0.5$ )

Table 2 Overview of Specimens

Specimen	$f_c'$	Web Reinforcement
	(MPa)	Ratio
		$\rho_w$ (%)
B2	36.2	0.0
B2-S	30.0	0.0
B3-S	30.0	0.4
B4-S	30.0	0.8

### 4. ANALYSIS OF B2 DEEP BEAM

#### 4.1 Experimental Test Results

Experimental load displacement graph of B2 is given by dashed line in Figure 7. The crack pattern and propagation is given in Figure 8.1 [3,4]. It was reported that, the first shear crack occurred initiating from the middle of the support plate (Figure 8.1.a) at  $P=525$  kN (a) (indicated as 'a' in Figure 7). Then, the diagonal crack propagated and a bending crack occurred at the

center of the span at  $P=800$  kN (b) shown in Figure 8.1.b. Diagonal cracks were connected and several fine cracks occurred near loading and support points in different directions due to compressive stress. At peak load  $P=1550$  kN (c), diagonal cracks developed and eventually concrete spalling was formed near loading and support plates with shear failure (Figure 8.1.c). At peak load, the crack width on the diagonal crack was measured as 0.25 mm.

#### 4.2 Comparison of Analytical and Experimental Results

Figure 7 shows the analytical load displacement curve indicated by solid line. Initial stiffness of analytical curve is higher than the experimental one. However, it agrees with the theoretical value calculated by Timoshenko beam theory. Analytical peak load is  $P=1722$  kN (C) that is slightly higher than the experimental one that is 1550 kN. The curves agreed significantly in post-peak region.

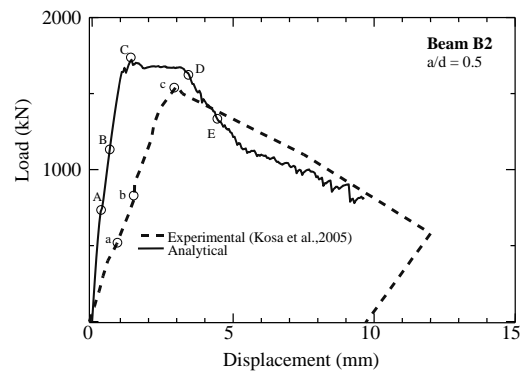


Fig. 7 Load Displacement Curves of B2

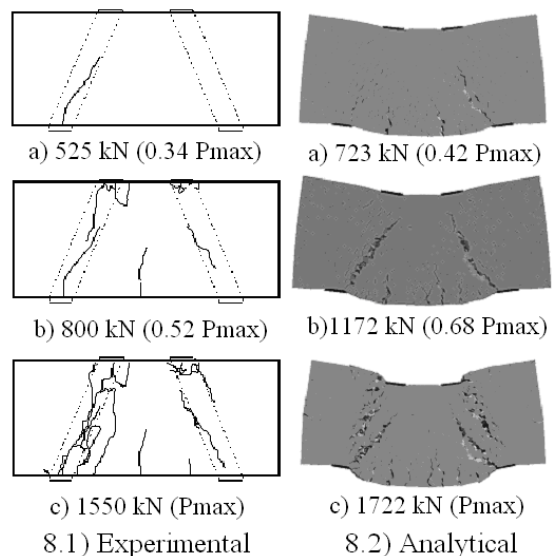


Fig. 8 Comparison of Crack Pattern

Figure 8.2 shows the crack pattern and propagation of numerical analysis. In the figures, magnification factors of deformation are 200, 100 and 40 respectively. At  $P=723$  kN, the shear crack becomes significant (Figure 8.2.a). The stiffness of the curve slightly changes at this point (A). Analytical and

experimental crack length and direction are similar and agreed well as shown. Similar behavior with experimental one is observed at  $P=1172$  kN (B) ( $0.68 P_{max}$ ) shown in Figure 8.1.b and 8.2.b. Main shear cracks extend outer side of loading plates and inner side of support plates towards to compression struts at the peak load (Figure 8.2.c). Thus, crack pattern is similar with the experimental one. That is, the length and directions of the inner and outer diagonal cracks agreed reasonably well. Moreover, the analytical crack width measured on the first diagonal crack is  $0.27$  mm at peak load, which is similar with the experimental one.

Consequently, RBSM results and experimental ones agreed reasonably well as discussed.

### 4.3 3D-Deformation of the Beam in Post-Peak Region

Failure mechanism can be investigated in detail by 3D-RBSM since it provides three-dimensional deformed shape. 3D deformed shapes are shown in Figure 9 at peak and post-peak loads. In order to indicate the failure behavior clearly, deformed shapes are magnified by factor of 40.

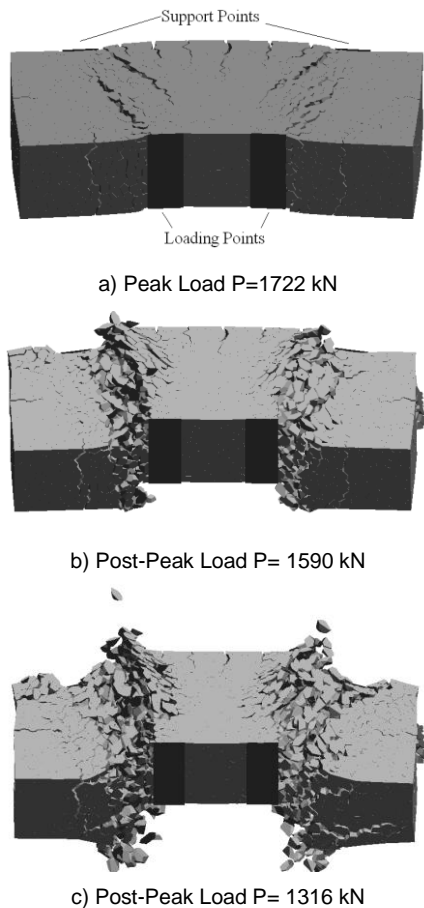


Fig. 9 3D Deformed Shapes

Spalling behaviour along the struts cannot be observed at peak load (Figure 9.a). However, spalling of concrete is formed along the struts just after the peak. 3D deformed shape at post-peak load  $P=1590$  kN (D) is shown in Figure 9.b. Lateral deformation increases in

post-peak region as shown. Flexural behavior is not observed. Figure 9.c gives 3D deformed shape at post-peak load  $P=1316$  kN (E). Comparison of the figures shows that, lateral deformation and concrete spalling increase in further post-peak loading steps.

### 4.4 Discussion on the Compression Strut

The principle stress distribution on the longitudinal middle section of the beam is shown in Figure 10. The maximum stress range in the figures is set to  $36.2$  MPa that is the compressive strength of concrete ( $f_c'$ ). Figure 10.a shows the stress distribution at pre-peak load  $P=1172$  kN (B). The strut initiation is shown in the figure.

Figure 10.b shows the stress distribution at peak load (C). The strut can be observed clearly in the figure. At post-peak load  $P=1316$  kN (E), the strut on the middle height of the beam is expanded significantly (Figure 10.c).

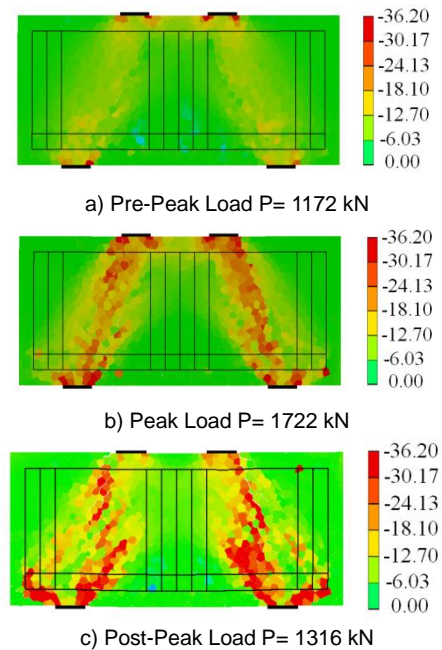


Fig. 10 The Principle Stress Distribution on the Longitudinal Middle Section

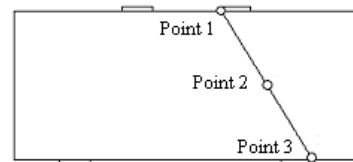


Fig. 11 Strut and Stress Measurement Points

Strut widths along the strut are compared. The widths are measured near loading point (Point1), middle height of the beam (Point 2) and support point (Point3) shown in Figure 11.

The comparison of normalized strut widths on point 1, 2 and 3 is shown in Figure 12. The widths are measured on both surface and middle longitudinal sections and compared in order to discuss of 3D effect in deep beam. The strut is determined by the area where

the stress is over  $0.5 f_c'$ . The measured widths are normalized by plate width.

The strut width at point 2 reaches more than 2.5 times of plate width on the surface section where it reaches to 3 times on the middle section. On the other hand, the widths at point 1 and 3 are around 1.5 times of the plate width on both middle and surface section.

In post-peak region, the strut disappears on surface section as shown in the figure. The reason is that concrete spalling occurs on the surface of the beam along the struts. On the other hand, the struts on the middle section is observed up to post-peak load  $P=1109$  kN.

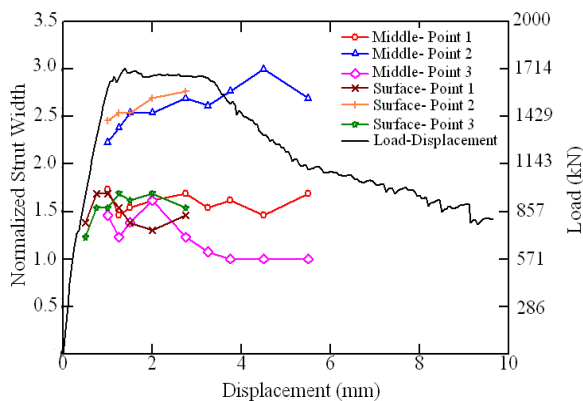


Fig. 12 The Comparison of Strut Widths

#### 4.5 Discussion of Compressive Stress

An important issue in deep beams is high complex stress state that localizes especially near loading and support points and within the compression strut (see Figure 10).

The change of the normalized principle stress along the compression strut is given in Figure 13. The measured stress values are normalized by  $f_c'$ . The stress is measured on three points shown in Figure 11. Moreover, the stress values measured on both the middle and surface longitudinal sections are compared and discussed in order to investigate 3D effects in deep beams.

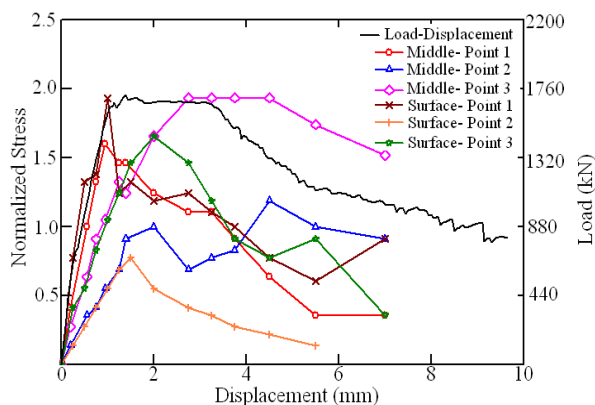


Fig. 13 The Change of the Stress

In pre-peak region, the stress values for both surface and middle section are similar as shown in the figure. Therefore, 3D effect is not observed in that region.

At point 1, the stress reaches to about 1.6 times of  $f_c'$  on the middle section and it is  $2.0 f_c'$  on the surface section near the peak load. Afterwards, the stress on the surface section decreases suddenly due to spalling of concrete on the beam surface. However, the stress on the middle section decreases gradually after peak stress.

At point 2, the stress on the middle section reaches to the compressive strength of concrete at the peak load and it is also about  $f_c'$  in post-peak region. On the other hand, the stress on the surface section gradually decreases in the post-peak region as distinct from the middle section case.

At Point 3, the stress on both the middle and surface section increases similarly up to the peak load as mentioned before. At the peak load, stress values are 45 MPa ( $1.24 f_c'$ ) and 53 MPa ( $1.46 f_c'$ ) on the middle and surface section respectively. However, the middle and surface sections show different behavior in post-peak region. On the middle section, the stress continues to increase after the peak load and finally it reaches up to 70 MPa ( $1.93 f_c'$ ). However, the stress on the surface section starts to decrease just after the peak. The reasons of the different behavior between surface and middle sections are confining effect in the middle part of the beam and concrete spalling on the surface.

As a result, 3D effect is important for deep beams having  $a/d=0.5$  especially in post peak-region. Moreover, 3D-RBSM can simulate 3D behavior reasonably as demonstrated and therefore it is a useful tool to seek the failure mechanism of deep beams in detail.

#### 5. THE EFFECT OF WEB REINFORCEMENT IN DEEP BEAMS WITH $a/d=0.5$

The effect of web reinforcement in deep beams having the shear span ratio of 0.5 is investigated in this chapter. In this purpose, three deep beams, which are B2-S, B3-S and B4-S, are analyzed. B2-S has no web reinforcement in shear span. On the other hand, B3-S and B4-S have the web reinforcement ratio of 0.4 % and 0.8 % respectively. The same concrete properties were used for three specimens in order to investigate the effect of web reinforcement purely. Details of the specimens were given in the chapter 3 (see Figure 4, 5 and 6 and Table 2).

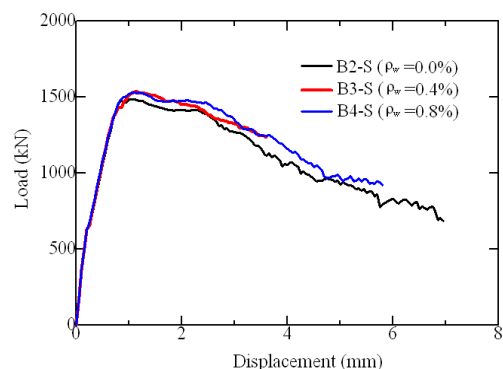


Fig. 14 The Comparison of Load-Displacement Curves

The comparison of load-displacement curves for B2-S (0.0%), B3-S (0.4%) and B4-S (0.8%) is shown in Figure 14. The curves are the same in pre-peak and so similar in post-peak region. The peak loads for B2-S, B3-S and B4-S are 1484 kN, 1534 kN and 1532 kN respectively that are very close. Therefore, there is almost no effect of the web reinforcement on load carrying capacity in deep beams with  $a/d=0.5$ . The cracking pattern, deformation and stress distribution are also the same for each case.

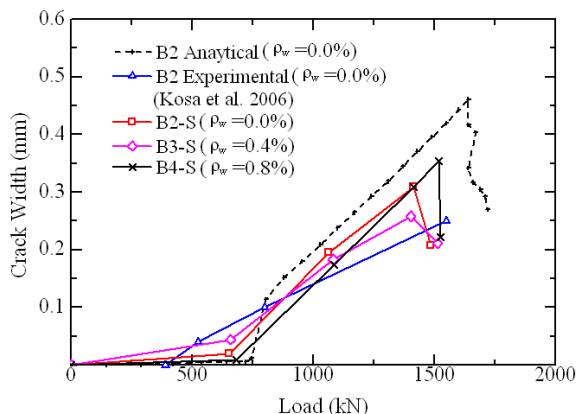


Fig. 15 The Comparison of Crack Widths

Figure 15 shows the comparison of crack widths for deep beams without and with web reinforcement in shear span. The widths are measured on the diagonal cracks at the middle height of the beam. The figures are similar for all cases as seen. It is understood that, web reinforcement arrangement has no significant effect on the crack growth rate and crack width.

The maximum strains of web reinforcement in shear span are measured. The strain values are 0.00093 and 0.00072 for B3-S (0.4%) and B4-S (0.8%) respectively. Therefore, the web reinforcement does not yield that shows it is not useful.

As a result; numerical analysis performed by RBSM shows that, there is no significant effect of web reinforcement in deep beams having the shear span ratio of 0.5.

## 6. CONCLUSIONS

- (1) 3D-RBSM is used in order to analyze deep beams without web reinforcement and having the shear span ratio of 0.5. The numerical results such as load displacement graphs and crack pattern are compared with the experimental ones. 3D-RBSM results show reasonable agreement with the experimental ones. It is shown that, 3D RBSM is a convenient tool for the analysis.
- (2) Three dimensional behavior in pre- and post-peak regions is investigated in deep beams without web reinforcement and having  $a/d=0.5$ . In order to investigate 3D effects, the strut widths and stress values along the strut are compared on both the middle and surface longitudinal sections. Due to spalling of concrete, the strut cannot be observed on the surface section after early

post-peak loads where it is shown until the further loads on the middle section. Moreover, the stress state on the middle and surface sections is distinct because of confinement effect in the middle beam section and spalling behavior on the surface. It is shown that, 3D effect is important in deep beams having  $a/d=0.5$ . Furthermore, three-dimensional behavior can be simulated by 3D-RBSM reasonably.

- (3) The effect of web reinforcement in deep beams with  $a/d=0.5$  is investigated. Deep beams with and without web reinforcement in shear span are compared and discussed. The load displacement graphs and crack growth rates are similar for both cases independent of the web reinforcement ratio. Thus, there is no significant effect of web reinforcement in deep beams that have the shear span ratio of 0.5.

## REFERENCES

- [1] T. Kawai: New Discrete Models and Their Application to Seismic Response Analysis of Structures, Nuclear Engineering and Design 48: 207-229, 1978
- [2] Y. Yamamoto, H. Nakamura, I. Kuroda & N. Furuya: Analysis of Compression Failure of Concrete by Three Dimensional Rigid Body Spring Model, Doboku Gakkai Ronbunshuu 64(4): 612-630, 2008 (In Japanese)
- [3] K. Kosa, Y. Umemoto, T. Nishioka, & H. Kobayashi: Experimental Studies on Failure Mode in the Deep Beam, Journal of Structural Engineering-JSCE 51A: 1283-1290, 2005 (In Japanese).
- [4] K. Kosa, T. Wakiyama, T. Nishioka & H. Kobayashi: Effect of Shear Span Ratio on the Fracture of Deep Beams, Doboku Gakkai Ronbunshuu E 62(4): 798-814, 2006 (In Japanese)
- [5] J. E. Bolander, G. S. Hong, & K. Yoshitake: Structural Concrete Analysis Using Rigid-Body-Spring Networks, Computer-Aided Civil and Infrastructure Engineering 15: 120-133, 2000
- [6] J. E. Bolander, G. S. Hong: Rigid-Body-Spring Network Modeling of Prestressed Concrete Members, ACI Structural Journal 99 (5): 595-604, 2002
- [7] S. Saito: Fracture Analyses of Structural Concrete Using Spring Networks With Random Geometry, PhD Dissertation, Kyushu University, 1999